Aircraft Engineering and Aerospace Technology

Emerald Article: A directional control system for UCAV automatic takeoff roll

Yunpeng Zhang, Haibin Duan

A directional control system for UCAV automatic takeoff roll

Yunpeng Zhang
Science and Technology on Aircraft Control Laboratory, School of Automation Science and Electrical Engineering, Beihang University, Beijing, People's Republic of China, and

Haibin Duan
Science and Technology on Aircraft Control Laboratory, School of Automation Science and Electrical Engineering, Beihang University, Beijing, People's Republic of China and
Science and Technology on Electro-Optic Control Laboratory, Luoyang, People's Republic of China

Abstract

Purpose – The purpose of this paper is to develop a directional and roll control system for unmanned combat air vehicle (UCAV) automatic takeoff roll, with the objective of keeping the UCAV along the runway centerline and keeping the wings level, especially when there is a crosswind.

Design/methodology/approach – The nonlinear model of the UCAV during takeoff roll is established. The model is linearized about the lateral-directional equilibrium point at different forward speeds. The approximate directional model and roll model are extracted using time-scale decomposition technique. Then the directional control law and roll control law are developed using gain scheduling approach. Nose wheel steering, differential brake and rudder are used as the primary directional control device at low, medium and high speeds, respectively, according to both the qualitative and quantitative analysis of their control effectiveness at different speeds. A priority matrix is developed to determine the secondary control device which is used if the primary control device fails, thus the directional control system can have a certain degree of fault tolerance.

Findings – This work developed the directional control law and roll control law by using gain scheduling approach. Experimental results verified that the developed directional and roll control system has high robustness and satisfactory fault tolerance: it can guarantee a safe takeoff under a 50 ft/sec crosswind, even if one directional control device fails, which satisfies the relevant criteria in MIL-HDBK-1797.

Practical implications – The directional and roll control system developed can be easily applied to practice and can steer the UCAV during takeoff roll safely, which will considerably increase the autonomy of the UCAV.

Originality/value – The paper shows how time-scale decomposition technique is employed to extract the approximate directional model and roll model, which simplifies model analysis and control law design. A fault-tolerant directional control system is designed to improve safety during takeoff.

Keywords Control systems, Dynamics, Aircraft engineering, Aircraft navigation, Unmanned combat air vehicle, Takeoff roll, Aircraft ground dynamics, Automatic takeoff control, Directional control, Time-scale decomposition

Paper type Research paper

Introduction

Unmanned combat air vehicles (UCAV) will play an important role in future aerial warfare (Duan *et al.*, 2010, 2011). Due to the elimination of human pilots, UCAVs can have a larger combat radius, greater payload, lower observability and higher manoeuvrability (Pradeep, 2002; Zhao and Lu, 2012). Moreover, compared with current manned platforms, UCAVs are more affordable and suitable for high-risk missions (Wise, 2003; Zhang *et al.*, 2010).

One of the main challenges of UCAV design is the automatic flight control system, and the automatic takeoff and landing control system is a key issue in UCAV control system design. This is because in all flight phases, the takeoff phase and landing phase are of the most importance and most aircraft disasters occur during these two phases. Therefore, a fully autonomous UCAV should be equipped with a well-adjusted and robust flight control system which can safely steer the vehicle during takeoff and landing (Brinker, 2004).

In this work, we will focus on UCAV autonomous takeoff, and only the takeoff roll phase will be studied. During takeoff roll, a UCAV accelerates itself on the ground until its speed reaches the rotation speed. The takeoff roll phase is quite distinct from the airborne phase, because during takeoff roll the ground exerts several kinds of forces on the UCAV, and these forces will largely determine the dynamics of the UCAV.

Many researchers and engineers have studied the aircraft ground dynamics and automatic takeoff control. Goto *et al.* (2001) developed a ground taxi control law for automatic landing of an unmanned vehicle. The function of the ground taxi controller is to stabilize the vehicle and keep it along the runway centreline until it stops. The directional control

The current issue and full text archive of this journal is available at **www.emeraldinsight.com/1748-8842.htm**

Aircraft Engineering and Aerospace Technology: An International Journal
85/1 (2013) 48–61

[DOI 10.1108/00022661311294076]

This work was partially supported by Natural Science Foundation of China (NSFC) under grant #61273054, #60975072 and #60604009, Program for New Century Excellent Talents in University of China under grant #NCET-10-0021, and Aeronautical Foundation of China under grant #20115151019.

Aircraft Engineering and Aerospace Technology: An International Journal
Volume 85 · Number 1 · 2013 · 48–61

devices are rudder and nose wheel steering, and the ailerons are also used to keep the wings level. Pradeep (2002) designed a longitudinal controller for UCAV automatic takeoff. The authors held that the aircraft is accelerating during takeoff and thus no longitudinal equilibrium point exists, about which the system can be linearized. Therefore, the longitudinal controller was designed based on the nonlinear longitudinal model using feedback linearization technique. The directional motion during takeoff was ignored in this paper. Duprez *et al.* (2004) developed a yaw rate controller of the aircraft during low speed roll on the ground. The controller was designed directly based on the nonlinear directional model using feedback linearization technique. After the controller design, the impact of the actuator dynamics and saturations and the controller robustness to friction uncertainty were also analyzed. Davidson (2004) described the autonomous flight control system of the UCAV X-45A, which can control and stabilize the vehicle through taxi, takeoff, flight and landing. The control system is divided into primary control architecture and control effector mixer: the primary control architecture generates the rotational acceleration command, and the control effector mixer distributes the command to different control devices. The ground yaw control devices are nose wheel steering, differential brake, elevons and thrust vectoring, which are used as primary control devices at different speeds according to their control effectiveness. The advantage of this control system is that it can easily accomplish the integrated control of multiple control devices. Yuan and Wang (2009) proposed an aircraft ground directional control law based on the interpolation online fuzzy control. Compared with a PID controller, the fuzzy controller can reduce the impact of the uncertainty of the model parameters. Xiong *et al.* (2009) designed a longitudinal control system for UAV automatic takeoff based on the active disturbance rejection control technique, which is used to estimate the wind disturbance and then compensate for it. The active disturbance rejection controller can effectively resist a downburst as well as horizontal and vertical wind turbulence, and therefore it can guarantee a safe takeoff in a wide range of wind conditions. Medici *et al.* (2012) described a faster and more reliable method to develop and validate the control laws of several UAV sub-systems, including the landing gear, nose wheel steering and wheel braking. It can verify the control laws in various failure conditions and thus allows more reliable and effective control logic to be produced. This method is applicable for the development of the UAV takeoff and landing control system.

In our work, the directional control system for UCAV autonomous takeoff roll will be emphasized. The main objective of our work is to design a directional control system to keep the UCAV along the centreline of the runway during takeoff roll, especially when there is a crosswind. Nose wheel steering, main wheel differential brake and rudder are used as the primary directional control device at low, medium and high speeds, respectively. In addition, the directional control system should also have a certain degree of fault tolerance: if one of the three control devices fails, the directional control system should be able to continue operating properly. The performance of the directional control system will be verified in computer simulations of UCAV crosswind takeoff roll, which should satisfy the relevant criteria stated in MIL-HDBK-1797.

In addition to the directional control, a roll control law is also designed to keep the wings level with the ailerons in case of large crosswinds. The longitudinal control law is not our focus in this work, but to accomplish the computer simulation, a simple longitudinal control law for takeoff roll is employed.

Model development

In this section, the mathematical model of the UCAV during takeoff roll is developed. During takeoff roll, the ground exerts forces on the landing gears of the UCAV, thus the model of the landing gears and the forces exerted by the ground will be emphasized (York and Alaverdi, 1996).

Oleo strut model

The oleo strut is approximated as a damped spring, and its mass is ignored. Thus, the force along the axis of the strut is:

$$F_{strut} = -k_{strut} \cdot \delta_{strut} - c_{strut} \cdot V_{strut} \quad (1)$$

where δ_{strut} is strut compression and V_{strut} is strut compression rate; k_{strut} is spring stiffness and c_{strut} is damping coefficient (Rankin, 2010; Hanke, 1971).

It is assumed that the nose gear strut and two main gear struts are all perpendicular to the ground, thus the force along the axis of each strut is vertical.

Tire model

When the UCAV is taxiing on the ground, the ground exerts vertical force, longitudinal force, side force, and rolling resistance on each tire of the UCAV.

Vertical force

The tire is approximately treated as a rigid body, and the mass of the wheel is ignored. Therefore, given the aforementioned assumption that all the three struts are perpendicular to the ground, we can obtain that the vertical force exerted by the ground on the tire is equal to the force along the axis of the strut.

Longitudinal force

When the main wheel brake is on, the ground will apply a longitudinal force (friction force) on the wheel and then the wheel will decelerate. The longitudinal force F_x is mainly determined by longitudinal slip ratio σ and tire normal load (vertical force) F_z (Pacejka, 2006).

Let V_x and ω denote the forward translational velocity and angular velocity of the wheel, then the longitudinal slip ratio is given by:

$$\sigma = \frac{V_x - \omega R}{V_x} \quad (2)$$

where R is the radius of the wheel.

The longitudinal slip ratio σ can be either positive or negative. When the brake is on, the angular velocity decreases and σ is positive. And when the UCAV is accelerating, σ is also positive.

The friction coefficient μ between the tire and the ground correlates closely with the longitudinal slip ratio σ. The Pacejka magic formula is adopted to approximate the relationship between μ and σ (Bakker *et al.*, 1987; Wang, 2001):

$$\mu = D\sin(Carctg(B\sigma)) \quad (3)$$

Here B, C and D are all constants which can be obtained according to experimental data.

Aircraft Engineering and Aerospace Technology: An International Journal
Volume 85 · Number 1 · 2013 · 48–61

In this work, the relationship between μ and σ is plotted in Figure 1.

As shown in Figure 1, when $\sigma = 0$, the wheel is in pure rolling condition and the friction coefficient is $\mu = 0$. When $\sigma = 1$, the wheel is in pure sliding condition but μ is not maximal at this point. μ reaches its maximum at a certain σ, which is defined as the optimal slip ratio.

After calculating the friction coefficient μ, the longitudinal force F_x is given by:

$$F_x = \mu \cdot F_z \tag{4}$$

Side force

Tire side force F_y is mainly determined by tire normal load (vertical force) F_z and slip angle α. Figure 2 shows the slip angle and side force of each tire (Duan, 2004).

For small slip angles, typically less than $\alpha = 5°$, the side force F_y has an approximate linear relationship with α (Rankin, 2010). The derivative of the side force with respect to the slip angle defines the tire cornering stiffness Y_α, and Y_α has a nonlinear relationship with tire normal load F_z (Klyde *et al.*, 2002).

According to Figure 2, the slip angle α of each tire can be calculated as follows (Duan, 2004).

The slip angle of the left main tire is:

$$\alpha_{ml} = -\arctan\left(\frac{v_{by} - r \cdot a_m}{v_{bx} + r \cdot b_w/2}\right) \tag{5}$$

and the slip angle of the right main tire is:

$$\alpha_{mr} = -\arctan\left(\frac{v_{by} - r \cdot a_m}{v_{bx} - r \cdot b_w/2}\right) \tag{6}$$

where v_{bx} and $v_{by}$are the components of UCAV ground speed along body x and y axes; r is the yaw rate; b_w is the distance between two main tires; a_m is the distance between a main tire to UCAV centre of gravity along body x-axis.

The nose wheel can be steered and let its deflection angle be θ_{nws}, thus the slip angle of the nose tire is:

$$\alpha_n = \theta_{nws} - \arctan\left(\frac{v_{by} + r \cdot a_n}{v_{bx}}\right) \tag{7}$$

Figure 1 The relationship between friction coefficient μ and longitudinal slip ratio σ

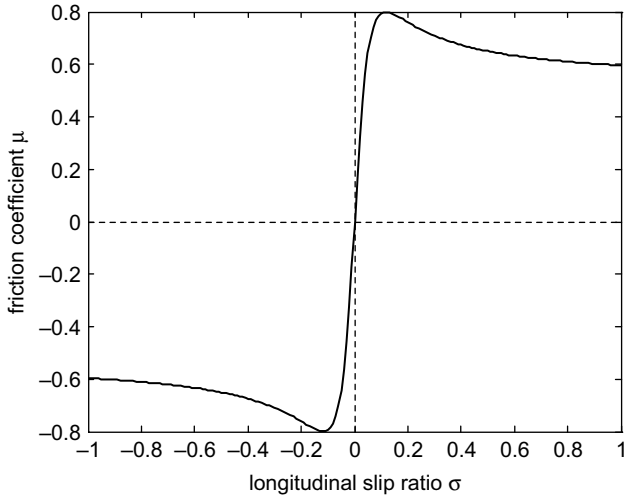

Figure 2 Slip angle and side force of each tire

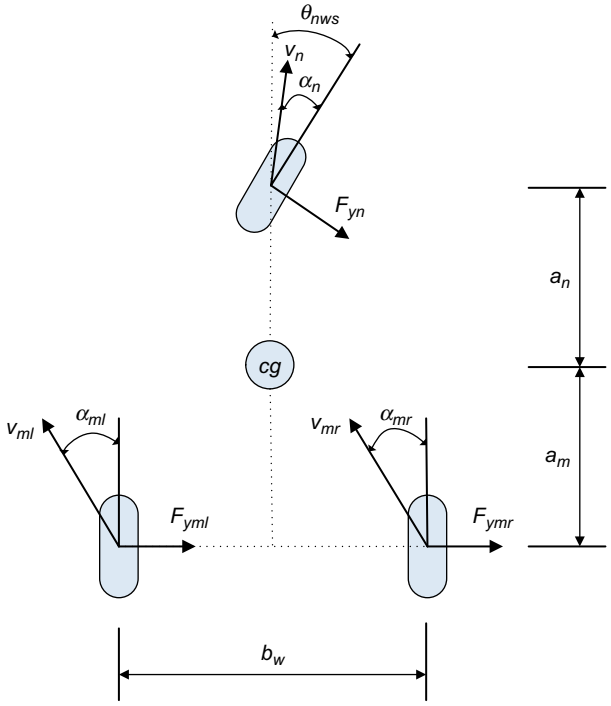

where a_n is the distance between the nose tire to UCAV centre of gravity along body x-axis.

Rolling resistance

The tire rolling resistance generates a moment on the wheel which is always in the opposite direction to the angular velocity of the wheel. The rolling resistance moment is calculated as:

$$M_r = \mu_r \cdot F_z \cdot R \tag{8}$$

where μ_r is the rolling resistance coefficient, and R is the radius of the wheel.

Brake system model

The UCAV is equipped with a main landing gear brake system, which can be used to accomplish both symmetrical brake and differential brake.

The mechanism by which the main landing gear brake affects the motion of the UCAV is as follows. When the brake of a main wheel is on, the brake system generates a brake torque on the main wheel, which makes the angular velocity of this main wheel decrease. This causes the aforementioned longitudinal slip ratio σ to become positive and thus the ground exerts a backward longitudinal force on the wheel, resulting in the deceleration of the UCAV.

Therefore, to model the above mechanism of the main landing gear brake, it is necessary to investigate the dynamics of the two main wheels.

During UCAV takeoff roll, the ground applies two moments on the main wheel: the moment generated by the longitudinal force and the rolling resistance moment. If the main landing gear brake is on, the brake system will also apply a brake torque on the main wheel. These moments determine the rotational motion of the main wheel. The longitudinal force is backward, thus it increases the angular velocity of the wheel; while the rolling resistance and the brake torque both

Aircraft Engineering and Aerospace Technology: An International Journal
Volume 85 · Number 1 · 2013 · 48–61

hinder the rotation of the wheel, thus they decreases the angular velocity of the wheel.

Let M_f denote the moment generated by the longitudinal force, M_r the rolling resistance moment, and M_b the brake torque, then the dynamics of the main wheel is given by:

$$\dot{\omega} = \frac{1}{I_w}(M_f - M_b - M_r) \tag{9}$$

where ω is the angular velocity of the wheel, and I_w is the moment of inertia of the wheel.

Complete model during takeoff roll

After modelling the landing gears, the complete nonlinear mathematical model of the UCAV during takeoff roll can be established. Here the main body of the UCAV is treated as a rigid body, while the oleo struts are approximated as damped springs. The mass of the oleo struts and wheels is ignored. In addition to the aforementioned forces exerted by the ground, there are also aerodynamic forces and moments, thrust force and gravity applied on the UCAV. Taking all these forces and moments into account, we can obtain the kinetics and kinematics equations of the UCAV during takeoff roll. The basic kinetics and kinematics equations of an aircraft can be found in all flight dynamics textbooks (Stevens and Lewis, 2003), thus they will not be repeated here.

Directional and roll control law design

Model linearization

The main objective of this work is to design a directional control law for takeoff roll, thus the first step is to linearize the nonlinear equations of motion about the lateral-directional equilibrium point and obtain the linear lateral-directional model during takeoff roll.

The takeoff roll phase is different from the airborne phase because the UCAV accelerates throughout takeoff roll, but flies at a constant speed most of the time when it is airborne. Thus, no steady state or equilibrium point exits in the longitudinal axis during takeoff roll because the forward speed keeps increasing. However, an obvious equilibrium point exits in the lateral and directional axes: if all the lateral-directional state variables and inputs keep zero and there is no crosswind, then this steady state will be maintained, thus this is the lateral-directional equilibrium point.

The nonlinear equations of motion during takeoff roll can then be linearized about this lateral-directional equilibrium point. At different forward speed, there is a corresponding linear lateral-directional model, which means that the linear lateral-directional model varies according to forward speed. At each forward speed, the longitudinal variables are frozen, while the lateral-directional variables are linearized. Therefore, the control gains which are designed based on the linear lateral-directional model will also vary according to forward speed, thus a gain scheduling approach should be employed to accomplish the directional control and roll control throughout takeoff roll.

A problem here is to determine the frozen longitudinal variables at one forward speed. It is not quite straightforward to determine the height of the centre of gravity and the pitch angle, because these two variables depend on the compressions of the three oleo struts. In this work, considering that the pitch angle is quite small, the height of the centre of gravity and the pitch angle can then be calculated approximately according to the following two equations:

1 The three strut vertical forces + aerodynamic lift = gravity.
2 The three pitch moments provided by strut vertical forces + aerodynamic pitch moment = 0.

The approximate compressions of the three struts can be calculated by solving these two equations, and then the approximate height of the centre of gravity and pitch angle can be calculated based on the compressions of the three struts. After determining these frozen longitudinal variables, the linear lateral-directional model can be obtained.

The state variables of the linear lateral-directional model during takeoff roll are as follows: the component of ground speed along body y-axis Δv_{by}, the roll rate Δp, the yaw rate Δr, the yaw angle $\Delta\psi$, the roll angle $\Delta\phi$, the lateral offset from the runway centreline Δy, the angular velocity of the left main wheel $\Delta\omega_{ml}$ and the angular velocity of the right main wheel $\Delta\omega_{mr}$.

The inputs of the linear lateral-directional model during takeoff roll are as follows: the rudder deflection $\Delta\delta_r$, the nose wheel deflection angle $\Delta\theta_{nws}$, the brake torque on the left main wheel ΔM_{bml}, the brake torque on the right main wheel ΔM_{bmr}, the aileron deflection $\Delta\delta_a$ and the crosswind speed ΔV_w.

Therefore, the linear lateral-directional model is given by:

$$\Delta\dot{X} = A\Delta X + B\Delta U \tag{10}$$

where:

$$\Delta X = (\Delta v_{by}, \Delta p, \Delta r, \Delta\psi, \Delta\phi, \Delta y, \Delta\omega_{ml}, \Delta\omega_{mr})^T \tag{11}$$

$$\Delta U = (\Delta\delta_r, \Delta\theta_{nws}, \Delta M_{bml}, \Delta M_{bmr}, \Delta V_w, \Delta\delta_a)^T \tag{12}$$

The lateral-directional state variables can be divided into three categories.

The variables that represent the directional motion are Δv_{by}, Δr, $\Delta\psi$, Δy, which are the main variables to be controlled by the directional control system to keep the UCAV along the runway centreline.

The variables that represent the roll motion are Δp, $\Delta\phi$, which are controlled by the roll control system to keep the wings level.

And the variables that represent the main wheel angular velocity are $\Delta\omega_{ml}$, $\Delta\omega_{mr}$. These two variables are necessary for modelling the main wheel differential brake control effect on the UCAV direction, because the differential brake will control the UCAV direction by the following mechanism: the differential brake applies a brake torque on one main wheel and causes the angular velocity of this main wheel to decrease, therefore the two main wheels will have different longitudinal slip ratios and thus the ground will exert asymmetrical longitudinal forces on the two main wheels, resulting in a yaw motion of the UCAV.

Approximate directional model and roll model

It is not convenient to use this complete linear lateral-directional model directly to design the directional control law and roll control law, especially when a state-space design technique is adopted. Therefore, the complete linear lateral-directional model should be decomposed and thus the approximate directional dynamics and roll dynamics can be extracted.

It is noted that the state variables $\Delta\omega_{ml}$ and $\Delta\omega_{mr}$ vary much faster than the other state variables, thus the complete linear lateral-directional model can be decomposed based on time scale (Chow and Kokotovic, 1976). The variables

Aircraft Engineering and Aerospace Technology: An International Journal
Volume 85 · Number 1 · 2013 · 48–61

$\Delta X_1 = (\Delta v_{by}, \Delta p, \Delta r, \Delta\psi, \Delta\phi, \Delta y)^T$ are considered as the slow variables in the model, while the variables $\Delta X_2 = (\Delta\omega_{ml}, \Delta\omega_{mr})^T$ are considered as the fast variables, then the complete linear lateral-directional model can be rewritten as:

$$\begin{aligned} \Delta\dot{X}_1 &= A_{11}\Delta X_1 + A_{12}\Delta X_2 + B_1\Delta U \\ \Delta\dot{X}_2 &= A_{21}\Delta X_1 + A_{22}\Delta X_2 + B_2\Delta U \end{aligned} \tag{13}$$

When ΔX_1 start to vary, ΔX_2 has finished varying. Thus, let $\Delta\dot{X}_2$ be zero, then we obtain:

$$A_{21}\Delta X_1 + A_{22}\Delta X_2 + B_2\Delta U = 0 \tag{14}$$

If A_{22} is nonsingular, we have:

$$\Delta X_2 = A_{22}^{-1}(-A_{21}\Delta X_1 - B_2\Delta U) \tag{15}$$

Substituting ΔX_2 into equation (13), we obtain:

$$\Delta\dot{X}_1 = (A_{11} - A_{12}A_{22}^{-1}A_{21})\Delta X_1 + (B_1 - A_{12}A_{22}^{-1}B_2)\Delta U \tag{16}$$

This is the approximate model of the slow variables Δv_{by}, Δp, Δr, $\Delta\psi$, $\Delta\phi$, Δy.

The above slow-variable model has both directional variables Δv_{by}, Δr, $\Delta\psi$, Δy and roll variables Δp, $\Delta\phi$, thus we should continue to decompose it to extract the directional dynamics and roll dynamics.

Considering that the roll variables vary faster than the directional variables, we can separate the directional dynamics and roll dynamics by employing the above time-scale decomposition technique again. In this approach, the approximate directional model and roll model can be obtained.

Let us take the linear lateral-directional model linearized at a forward speed of 100 ft/s as an example. The complete model is given in the Appendix. The poles of the complete model are:

$$\begin{aligned} \lambda_1 &= 0 \\ \lambda_2 &= 0 \\ \lambda_3 &= -25.177 \\ \lambda_4 &= -22.396 \\ \lambda_5 &= -22.139 \\ \lambda_6 &= -4.416 \\ \lambda_{7,8} &= -1.300 \pm 0.165 \end{aligned} \tag{17}$$

Then we extract the approximate directional model and roll model from the complete model, and they are also given in the Appendix. The poles of the approximate directional model are:

$$\begin{aligned} \lambda_{d1} &= 0 \\ \lambda_{d2} &= 0 \\ \lambda_{d3} &= -1.226 \\ \lambda_{d4} &= -1.380 \end{aligned} \tag{18}$$

The two poles located at zero represent the dynamics of $\Delta\psi$ and Δy, indicating that these two variables are in indifferent equilibrium. The other two poles -1.226 and -1.380 represent the dynamics of Δv_{by} and Δr, which determine the directional dynamic characteristics. We can observe that these two poles are a little different from the poles -1.300 ± 0.165 of the complete model, which is because the directional model is an approximation.

The poles of the approximate roll model are:

$$\begin{aligned} \lambda_{r1} &= -4.523 \\ \lambda_{r2} &= -25.273 \end{aligned} \tag{19}$$

These two poles determine the roll dynamic characteristics. The roll axis has high natural frequency and is well-damped, due to the high spring stiffness and damping coefficient of the oleo strut.

Directional control law design

On the basis of the approximate directional model, the directional control law can be developed. In this work, the directional control laws for nose wheel steering, differential brake and rudder are designed separately, which means each control device has its own control law.

First the structure of the control law should be determined. The lateral offset Δy is the main variable to be fed back and controlled to keep the UCAV along the runway centreline. The integral of Δy should also be fed back to eliminate the steady-state error when there is a constant crosswind. In addition, the lateral velocity Δv_{by}, the yaw rate Δr and the yaw angle $\Delta\psi$ will all be fed back to improve the dynamic characteristics (Cotter and Cohen, 1977).

After determining the structure of the control law, we should then adjust the feedback gains. To determine the gains, several techniques can be applied, such as root *locus* method and LQR method. We have mentioned that the linear lateral-directional model varies according to forward speed, thus the control gains which are designed based on the linear lateral-directional model will also vary with forward speed. Simulation results show that it is impossible to accomplish the directional control for the whole process of takeoff roll if the control gains are not adjusted according to forward speed, especially when there is a crosswind. Therefore, the gain scheduling approach should be employed: the control gains at a series of forward speeds will be designed and the others will be calculated by linear interpolation.

Note that if only one control device (nose wheel steering or differential brake or rudder) is providing the directional control and there is a constant crosswind, then the ground speed and the UCAV heading cannot be controlled to be parallel to the runway centreline at the same time. This can be explained as follows: if both the ground speed and the UCAV heading are parallel to the runway centreline, then the slip angle of each wheel is zero, thus the ground will not exert side force on any wheel. However, the crosswind will apply both a side force and a yaw moment on the UCAV, thus if only one control device is providing the directional control, this control device cannot balance both the side force and the yaw moment at the same time. Therefore, the ground speed and the UCAV heading cannot be controlled to be parallel to the runway centreline at the same time. In this work, the main objective is to eliminate the lateral offset, thus the ground speed will be controlled to be parallel to the runway centreline, and therefore there will be a small angle between the UCAV heading and the runway centreline if there is a crosswind.

Roll control law design

During takeoff roll, the roll axis shows high natural frequency and damping, due to the high spring stiffness and damping

Aircraft Engineering and Aerospace Technology: An International Journal
Volume 85 · Number 1 · 2013 · 48–61

coefficient of the oleo strut, thus the dynamic characteristics of the roll axis do not need to be improved. The function of the roll control system is to keep the wings level when there is a large crosswind. The roll angle $\Delta\phi$ and its integral are fed back to eliminate the steady-state roll angle under constant crosswind, and the roll rate Δp is also fed back to increase damping.

Directional control allocation

Primary directional control devices at different speeds

During takeoff roll, the UCAV keeps accelerating. At low speeds, the aerodynamic forces are weak while the forces exerted by the ground are relatively strong. As the forward speed increases, the aerodynamic forces become stronger, while the forces exerted by the ground become weaker due to the increase of the lift. Therefore, it is necessary to divide the takeoff roll into three phases: low speed phase, medium speed phase and high speed phase (Davidson, 2004; Mazur, 2002).

Nose wheel steering is used as the primary directional control device in low speed phase, because the nose wheel deflection can cause a large side force due to the large vertical force provided by the ground. In medium and high speed phase, the side force caused by nose wheel deflection is relatively weak because of the decrease of the vertical force, thus nose wheel steering is not used as the primary directional control device at medium and high speeds. Another reason is that the actuator of nose wheel steering is not fast enough to provide control at high speeds.

Main wheel differential brake is used as the primary directional control device in medium speed phase. At medium speeds, the control effectiveness of the nose wheel steering is lowered, while the control effectiveness of the rudder is not high enough. Therefore, main wheel differential brake is primarily used in this phase because it can provide ample control power. At high speeds, the asymmetrical longitudinal forces caused by differential brake decrease due to the decrease of the vertical force, and the actuator of differential brake is also not fast enough to provide control at high speeds, thus differential brake is not used as the primary directional control device at high speeds.

Rudder is used as the primary directional control device in high speed phase. At high speeds, the aerodynamic forces are strong enough, thus the control effectiveness of the rudder is quite high.

A quantitative analysis is conducted to further illustrate the control effectiveness of the three directional control devices in different phases. In this work, the low speeds range from 0 to 30 ft/s, the medium speeds from 30 to 170 ft/s, and the high speeds from 170 to 350 ft/s. The rotation speed is 350 ft/s. To investigate the control effectiveness, we calculate the output needed by each device to keep the UCAV along the runway centreline under a constant crosswind of 50 ft/s. This calculation is based on the linear lateral-directional model, and the result is shown in Table I.

From Table I, we can observe that at low speeds, both the nose wheel deflection and differential brake torque needed to resist the crosswind are quite small, thus they can provide effective directional control; while the rudder deflection needed is much larger than the deflection available, indicating that its control effectiveness is quite low at low speeds.

At medium speeds, the nose wheel deflection and differential brake torque needed both increase, and differential brake is more effective than nose wheel steering. The rudder deflection needed becomes available, but its control effectiveness is still not high enough.

At high speeds, the nose wheel deflection needed is close to the deflection available, thus nose wheel steering has low control effectiveness. The differential brake and rudder can both provide effective directional control; however, considering that the brake actuator is relatively slow, the rudder will be used as the primary control device.

The primary directional control devices at different forward speeds are shown in Figure 3.

Switch between different control devices

Different primary directional control device will be used at low, medium and high speeds, thus a switch strategy should be designed to avoid a sudden signal transient. In this work, a one second linear fade is used to accomplish the control device switch (Davidson, 2004). Specifically, each control device has a weight coefficient ranging from 0 to 1, and the actual output of a device is the product of its weight coefficient and its nominal output calculated using the control law. Generally, the weight coefficient of the current primary control device is 1, while the weight coefficients of the other two devices are both 0, which means that only one control device is being used currently. During the transition phase, the primary directional control device will change from one to another. To accomplish a smooth transition, the two devices will be used simultaneously throughout the transition phase: the weight coefficient of the former device decreases linearly from 1 to 0, while the weight coefficient of the latter device increases linearly from 0 to 1. The duration of the transition phase is set to 1 s. At the end of the transition phase, the former device stops operating and the latter device obtains full authority.

The above description of the switch between different control devices during takeoff roll can be further illustrated by Figure 4.

Fault-tolerant directional control system

In normal circumstances, nose wheel steering, differential brake and rudder are used as the primary directional control device at low, medium and high speeds, respectively. In addition to this, our directional control system is also required to have a certain degree of fault tolerance: if one of the three control devices suddenly fails, the directional control system should be able to continue operating properly. To satisfy this requirement, we define a priority matrix to determine the secondary control device which is used if the primary control device fails. The development of the priority matrix is based on the aforementioned control effectiveness of each device at different speeds, and it is shown in Table II.

During takeoff roll, the UCAV will detect the fault signal of the primary control device to judge if it is operating properly. If the primary control device suddenly fails, the secondary control device will be used immediately. According to the aforementioned control effectiveness, the secondary control device can also provide effective directional control and guarantee a safe takeoff. In extreme cases, if both the primary control device and the secondary control device fail, then the last control device will be used. The last control device cannot provide enough control power, thus the control performance will be lowered; and the takeoff may be aborted if there is a large crosswind.

Table I Output needed by each device at different speeds to resist a constant crosswind

Directional control devices	Amount available	Amount needed at different forward speed Forward speed of 10 ft/s (low speed)	Forward speed of 100 ft/s (medium speed)	Forward speed of 300 ft/s (high speed)
Nose wheel deflection angle (deg)	4	0.19	1.77	3.63
Differential brake torque (lb × ft²/s²)	2×10^5	1.28×10^3	1.22×10^4	2.65×10^4
Rudder deflection (deg)	30	87.2	8.3	2.1

Figure 3 Primary directional control devices at different forward speeds

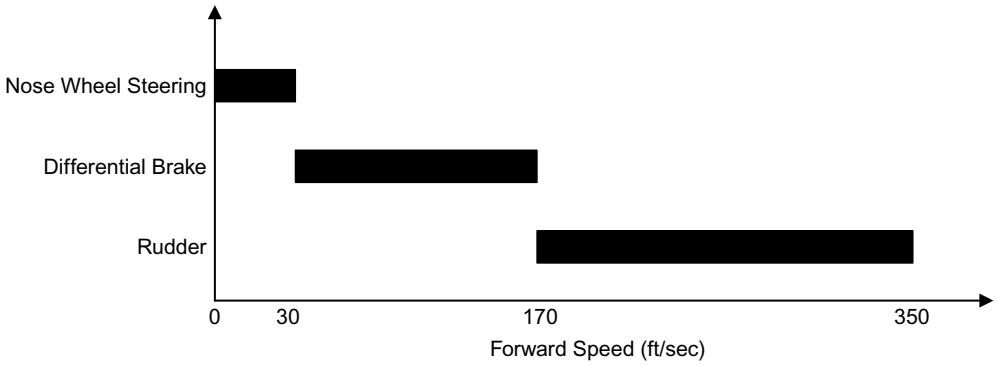

Figure 4 Switch between different control devices during takeoff roll

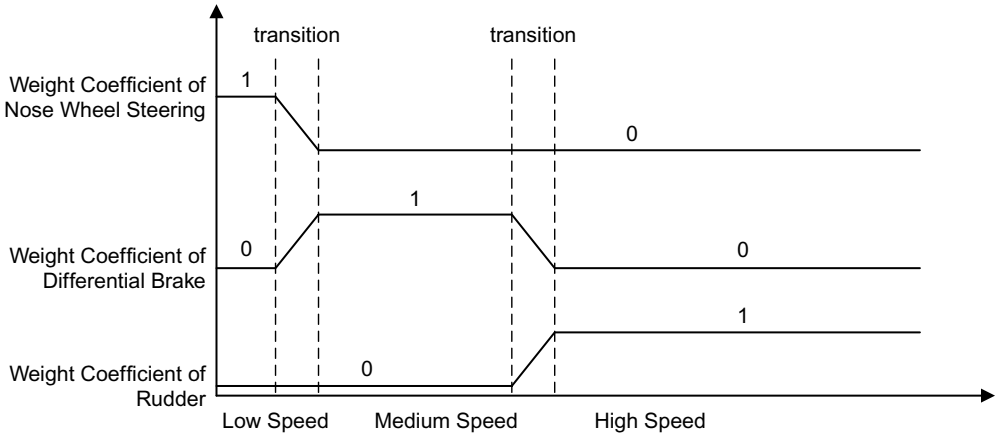

Table II Priority matrix of directional control devices

	Primary	Secondary	Last
Low speeds	Nose wheel steering	Differential brake	Rudder
Medium speeds	Differential brake	Nose wheel steering	Rudder
High speeds	Rudder	Differential brake	Nose wheel steering

Therefore, after obtaining the forward speed and the fault signal of the three control devices, the fault-tolerant directional control system will decide which control device should be used currently, following the decision procedure shown in Figure 5.

Simulation results

To evaluate the performance of the directional control system and roll control system, simulations of the whole process of the UCAV takeoff roll under crosswind are conducted. In addition to the normal condition, several failure conditions are also simulated to verify the property of fault tolerance.

The longitudinal control law is not our focus in this work, but to accomplish the simulation, a simple longitudinal control law for takeoff roll is employed: the UCAV is at full throttle throughout takeoff roll, and when its forward speed reaches the rotation speed, the elevator will be deflected to raise the nose, and this will be the end of takeoff roll.

Figure 5 Decision procedure of the fault-tolerant directional control system

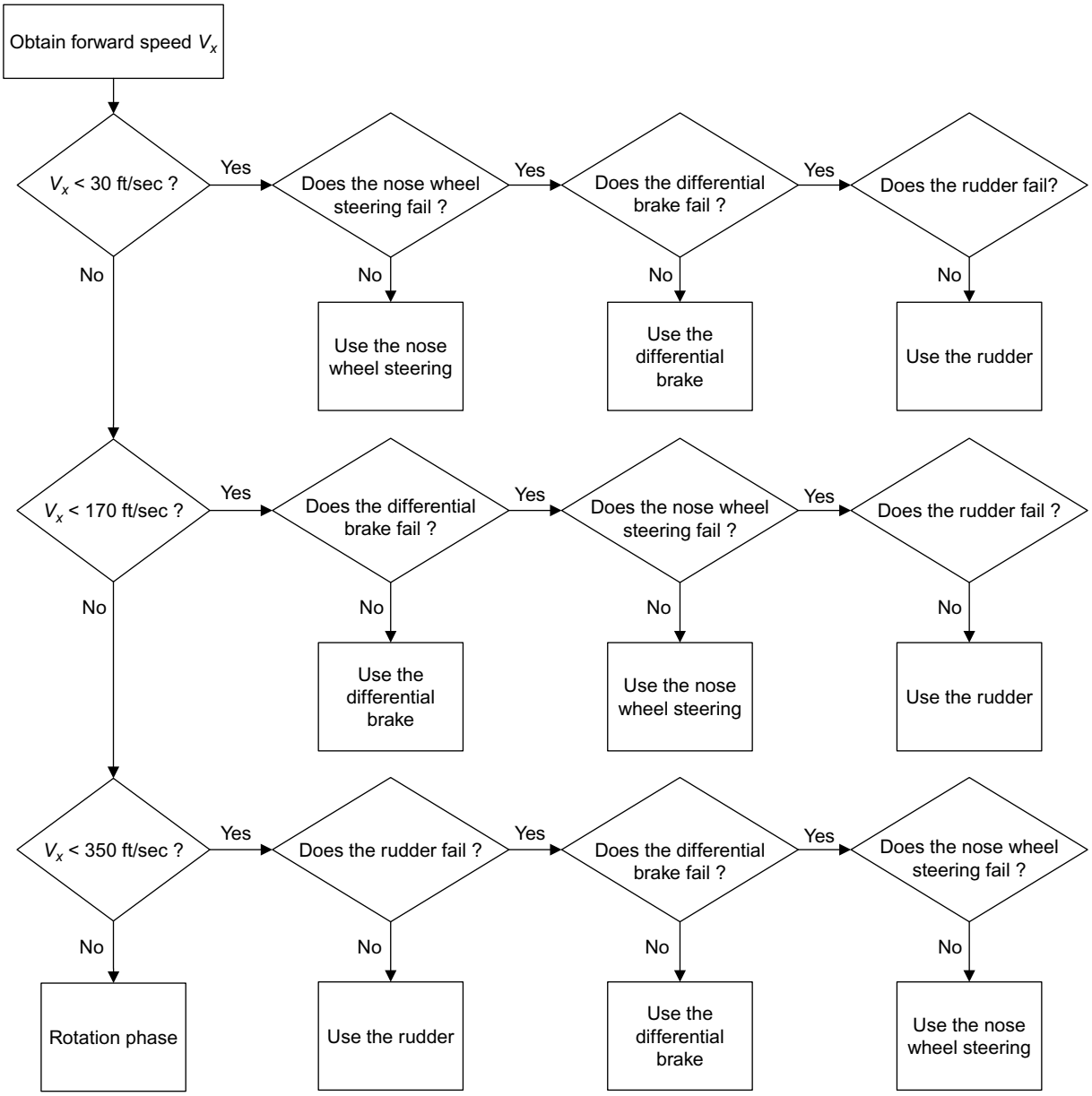

In the simulations, the low speeds range from 0 to 30 ft/s, the medium speeds from 30 to 170 ft/s, and the high speeds from 170 to 350 ft/s. The rotation speed is 350 ft/s. The crosswind is a 50 ft/s constant wind which is perpendicular to the runway centreline, and this satisfies the relevant criteria stated in MIL-HDBK-1797.

Normal condition simulation

The first simulation is a crosswind takeoff roll in normal condition without control device failure. The initial lateral offset of the UCAV is set to 0. The simulation results are shown in Figures 6 and 7: Figure 6 contains the response of the forward speed, the lateral offset, the heading and the roll angle, and Figure 7 contains the nose wheel deflection, the differential brake torque and the rudder deflection.

As shown in Figure 6, the lateral offset of the UCAV does not exceed 4 ft throughout takeoff roll. At low speeds the impact of the crosswind is relatively small, thus the lateral offset keeps around 0. As the forward speed increases, the impact of the crosswind becomes stronger, thus the lateral offset increases to about 4 ft. It is noted that the lateral offset is not controlled to 0 before rotation. This is because the forward speed keeps accelerating, thus the impact of the crosswind also keeps increasing. Moreover, the duration of takeoff roll is relatively short, thus it is difficult for the directional control system to reduce the lateral offset to 0 within such a short time.

It is observed that the UCAV heading also increases slowly as the forward speed increases. This is consistent with our previous analysis: the ground speed and the UCAV heading cannot be controlled to be parallel to the runway centreline simultaneously under crosswind. As forward speed increases,

Figure 6 Response of state variables in normal condition simulation

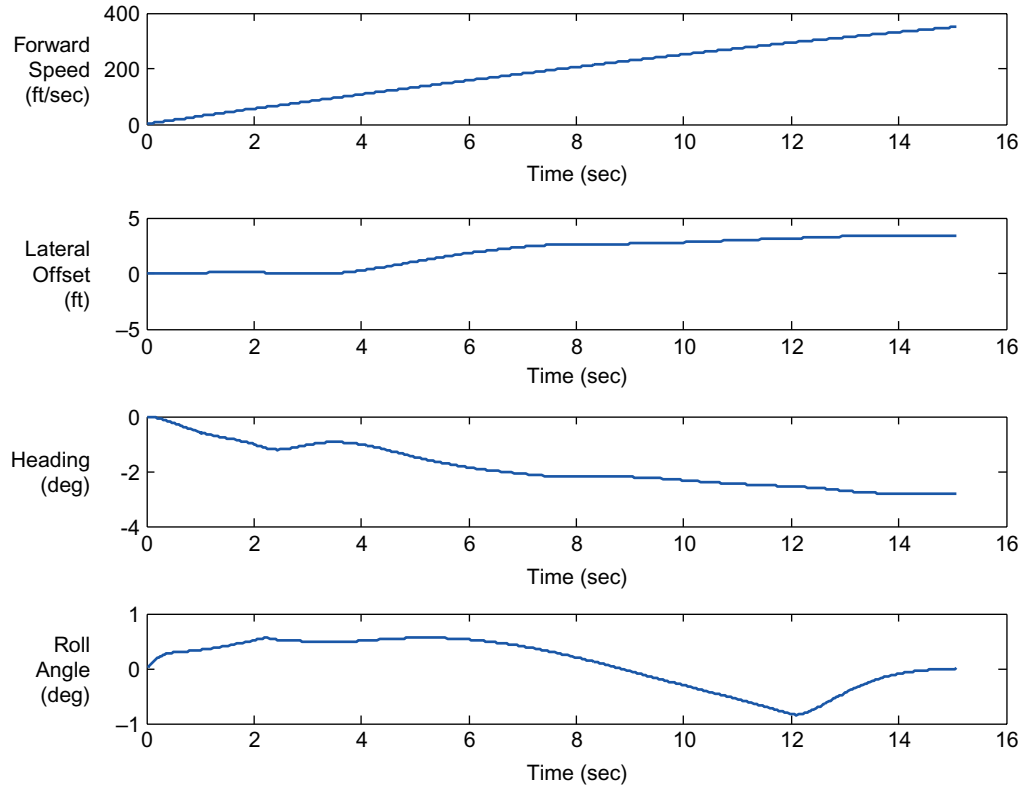

Figure 7 Input variables in normal condition simulation

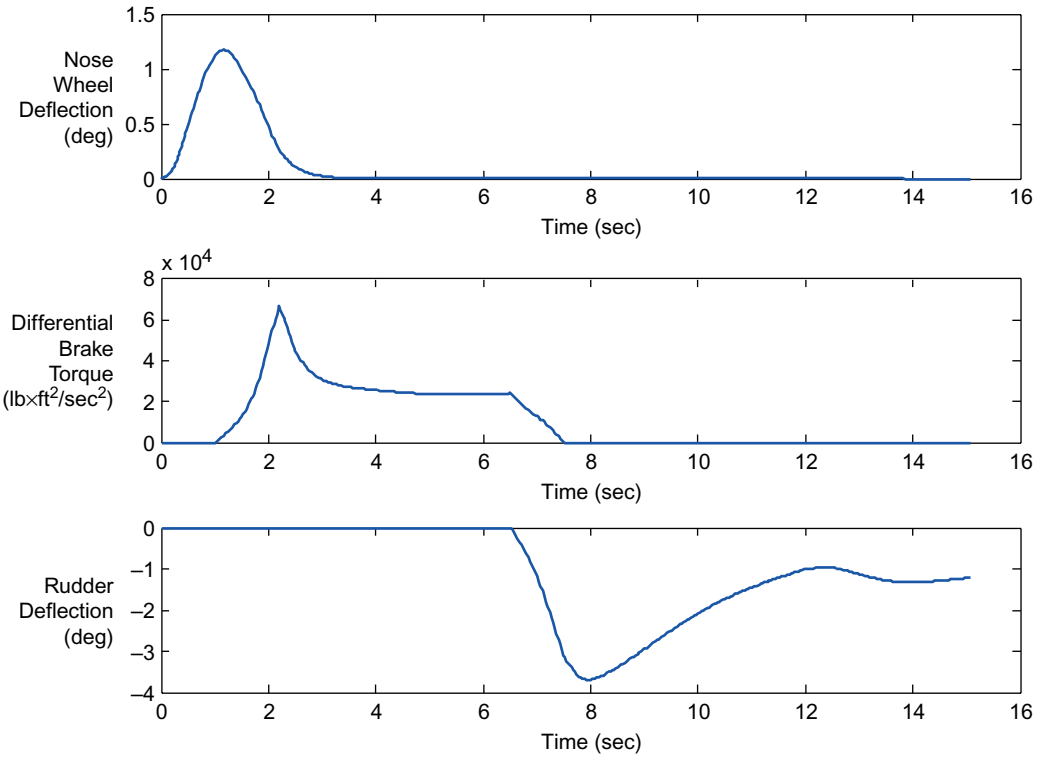

the impact of the crosswind becomes stronger, and the angle between the UCAV heading and the runway centreline also increase. However, this angle will not exceed 3°, and this is acceptable to the UCAV.

It is also observed that the roll control law limits the roll angle within 1°. Other simulations show that if there is no roll axis control, the roll angle will reach 2.5°.

Figure 7 shows that nose wheel steering, differential brake and rudder provide directional control at low, medium and high speeds, respectively, and the transition is smooth. Specifically, the forward speed reaches 30 ft/s at time = 1 s, 170 ft/s at time = 6.5 s, and 350 ft/s at time = 15 s. Thus, from time = 1 s to time = 2 s, the control device switches from nose wheel steering to differential brake; and from time = 6.5 s to time = 7.5 s, the control device switches from differential brake to rudder. The maximum nose wheel deflection and rudder deflection are about 1.2° and 4°, respectively, which are quite small. The maximum differential brake torque is about 6.5×10^4 lb × ft^2/s^2, which is also not large compared with the available differential brake torque.

Differential brake failure condition simulation

The second simulation is a crosswind takeoff roll in a failure condition. In this condition the differential brake suddenly fails when it is operating at medium speeds and according to the priority matrix, the nose wheel steering, which is the secondary control device, will be used immediately. The initial lateral offset of the UCAV is set to 0. Figures 8 and 9 show the state variables and input variables.

The differential brake suddenly fails at time = 4 s and the nose wheel steering is used immediately, but the nose wheel steering does not obtain full authority until time = 5 s. Thus, from time = 4 s to time = 5 s, the heading angle soon increases, which also causes the increase of the lateral offset. At time = 5 s, the nose wheel deflection reaches 4°, which is the maximum available nose wheel deflection, preventing further increase of the heading angle. Then from time = 6.5 s to time = 7.5 s, the control device switches from nose wheel steering to rudder, and the fluctuation of the lateral offset and heading has been suppressed. During the takeoff, the lateral offset is limited within 5 ft. The maximum rudder deflection reaches about 15°, which is much larger than that in normal condition, but is still acceptable.

Rudder failure condition simulation

The third simulation is also a crosswind takeoff roll in a failure condition. In this condition the rudder suddenly fails when it is operating at high speeds and according to the priority matrix, the differential brake, which is the secondary control device, will be used immediately. The initial lateral offset of the UCAV is set to 0. Figures 10 and 11 show the state variables and input variables.

The rudder suddenly fails at time = 10 s and the differential brake is used immediately. The fluctuation of the lateral offset and heading is not obvious, because the control effectiveness of the differential brake is also high enough at high speeds. The lateral offset is limited within 4 ft.

The two simulations in failure conditions show that the directional control system has a certain degree of fault tolerance: if the primary control device fails, the secondary control device can provide enough control power to resist the crosswind and guarantee a safe takeoff.

Figure 8 Response of state variables in differential brake failure condition simulation

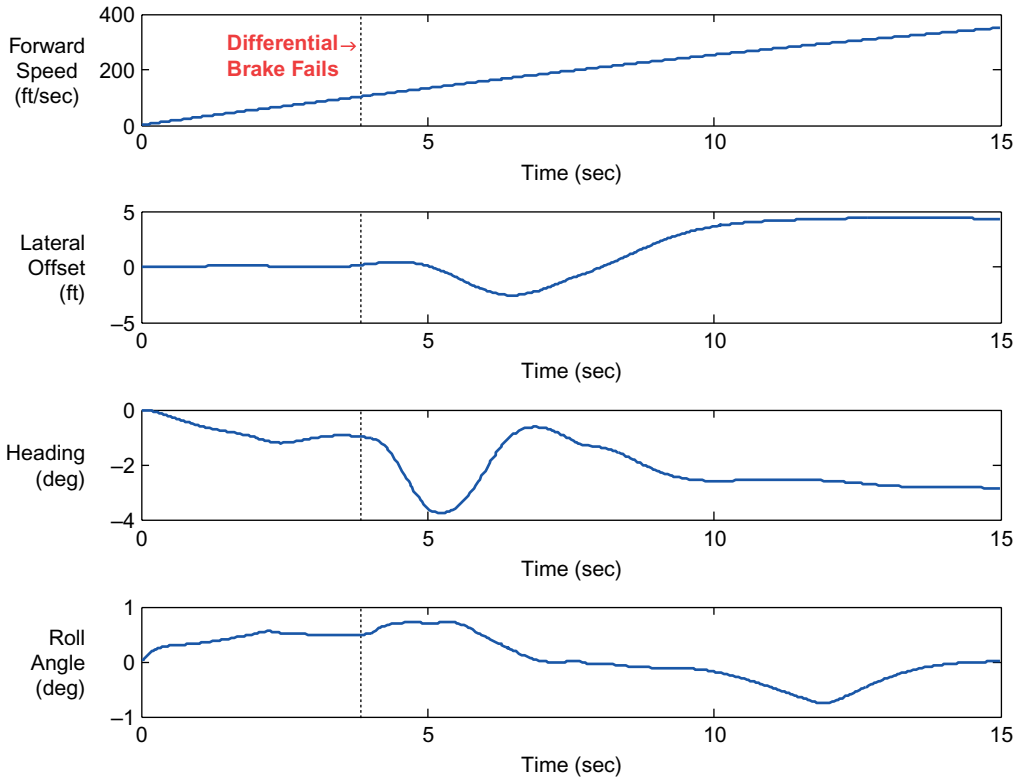

Figure 9 Input variables in differential brake failure condition simulation

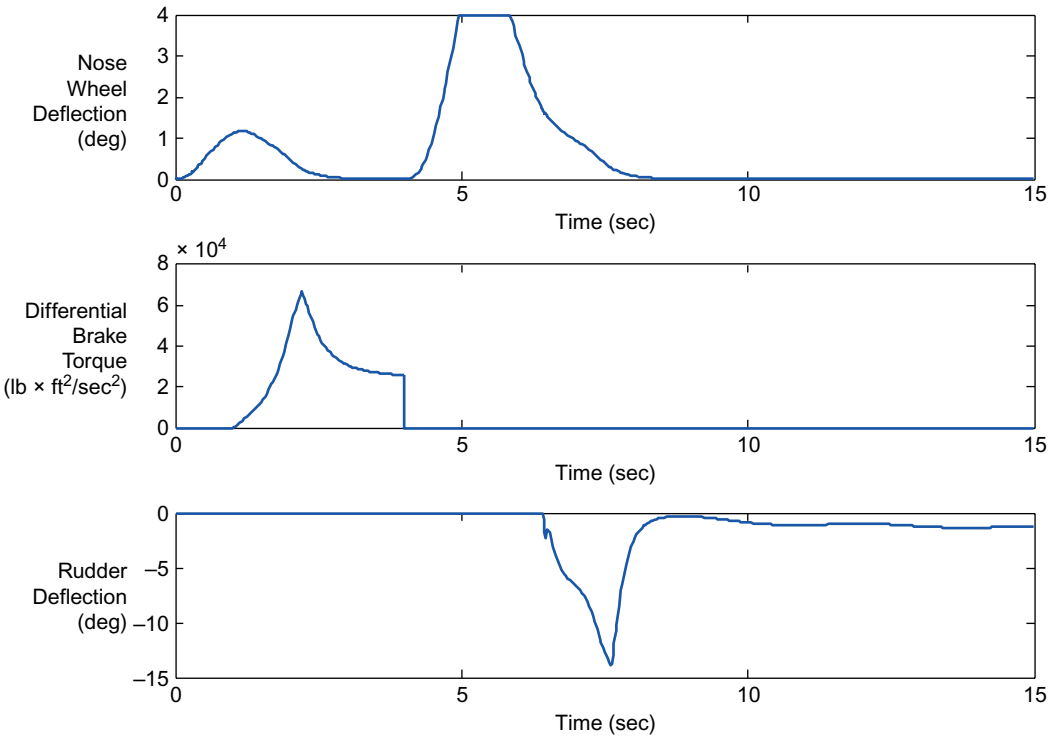

Figure 10 Response of state variables in rudder failure condition simulation

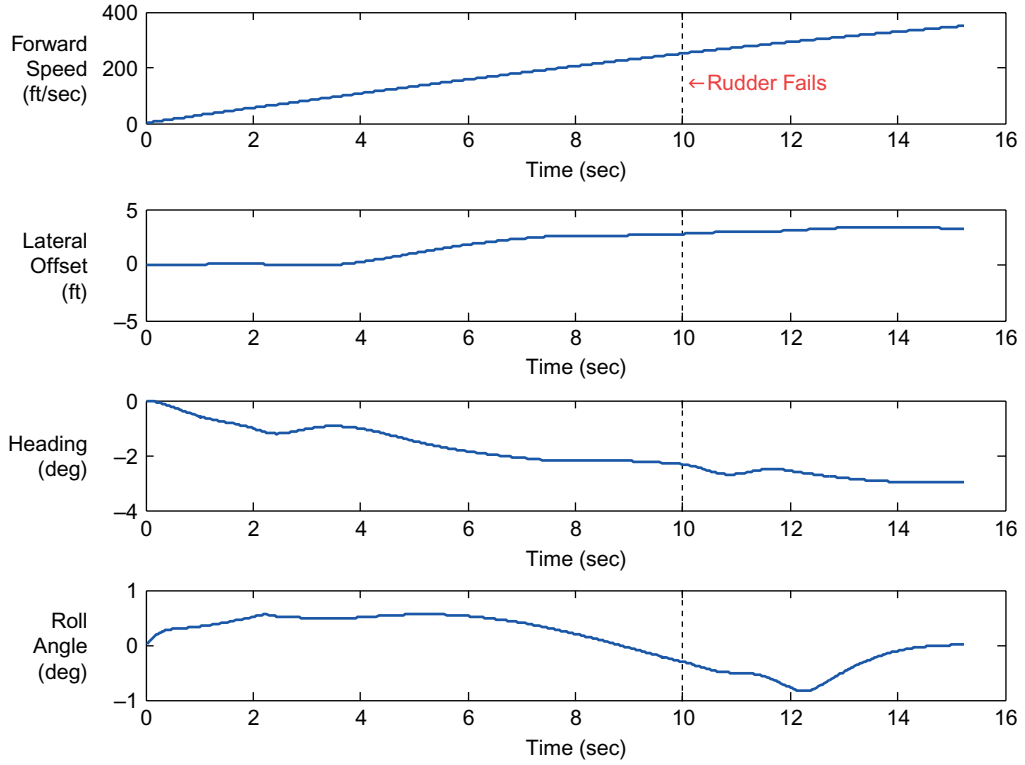

Figure 11 Input variables in rudder failure condition simulation

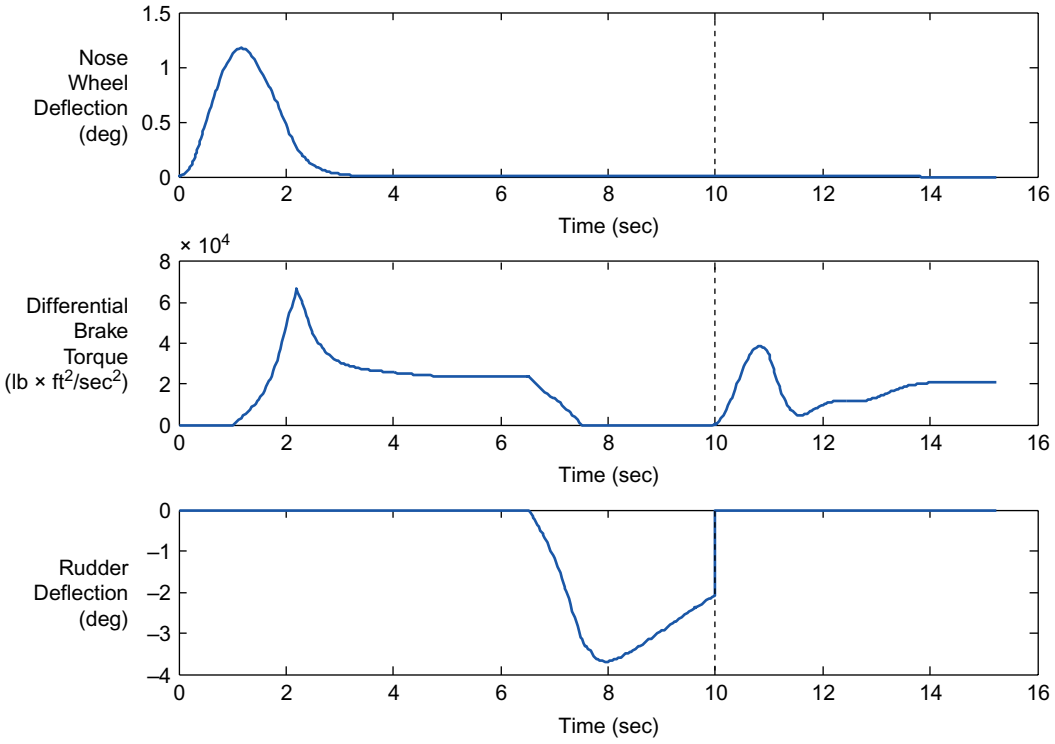

Conclusion

In this paper, a directional and roll control system is developed for UCAV automatic takeoff roll, with the objective of keeping the UCAV along the runway centreline and keeping the wings level, especially when there is a crosswind. The nonlinear mathematical model of the UCAV during takeoff roll is established. The model is linearized about the lateral-directional equilibrium point at different forward speeds. To further analyze the model and design the control law, the approximate directional model and roll model are extracted using time-scale decomposition technique and then the directional control law and roll control law are developed using gain scheduling approach. Nose wheel steering, main wheel differential brake and rudder are used as the primary directional control device at low, medium and high speeds, respectively, according to their control effectiveness at different speeds. A priority matrix is developed to determine the secondary control device which is used if the primary control device fails, thus the directional control system can have a certain degree of fault tolerance. Simulations in both normal condition and several failure conditions show that the directional and roll control system has high robustness and satisfactory fault tolerance: it can guarantee a safe takeoff under a 50 ft/s crosswind even if one directional control device fails, which satisfies the relevant criteria in MIL-HDBK-1797.

References

Bakker, E., Nyborg, L. and Pacejka, H.B. (1987), "Tyre modelling for use in vehicle dynamics studies", SAE Paper 870421.

Brinker, J. (2004), "Autonomous steering of the joint unmanned combat air systems (J-UCAS) X-45A", *AIAA 3rd "Unmanned Unlimited" Technical Conference, Workshop and Exhibit, Chicago, IL*, AIAA Paper 2004-6575, pp. 1-9.

Chow, J. and Kokotovic, P. (1976), "A decomposition of near-optimum regulators for systems with slow and fast modes", *IEEE Transactions on Automatic Control*, Vol. 21 No. 5, pp. 701-5.

Cotter, C.J. and Cohen, G.C. (1977), "Automatic rollout control of the 747 airplane", *Guidance and Control Conference, Hollywood, Florida*, American Institute of Aeronautics and Astronautics, New York, NY, pp. 483-91.

Davidson, R. (2004), "Flight control design and test of the joint unmanned combat air system (J-UCAS) X-45A", *AIAA 3rd "Unmanned Unlimited" Technical Conference, Workshop and Exhibit, Chicago, IL*, AIAA Paper 2004-6557, pp. 1-15.

Duan, H.B., Zhang, Y.P. and Liu, S.Q. (2011), "Multiple UAVs/UGVs heterogeneous coordinated technique based on receding horizon control (RHC) and velocity vector control", *Science China Technological Sciences*, Vol. 54 No. 4, pp. 869-76.

Duan, H.B., Shao, S., Su, B.W. and Zhang, L. (2010), "New development thoughts on the bio-inspired intelligence based control for unmanned combat aerial vehicle", *Science China Technological Sciences*, Vol. 53 No. 8, pp. 2025-31.

Duan, S.Y. (2004), "Modeling of an unmanned aerial vehicle during take-off/landing and flight dynamics simulation", Master's thesis, Tsinghua University, Beijing.

Duprez, J., Mora-camino, F. and Villaume, F. (2004), "Control of the aircraft-on-ground lateral motion during low speed roll and manoeuvers", *2004 IEEE Aerospace Conference Proceedings, Big Sky, MT, IEEE*, pp. 2656-66.

Goto, K., Miyazawa, Y. and Sagisaka, M. (2001), "Development of ground taxiing control law for automatic landing flight experiment (ALFLEX)", paper presented at AIAA Guidance, Navigation, and Control Conference and Exhibit, Montreal, Canada, AIAA Paper 2001-4242.

Hanke, C. (1971), *The Simulation of a Large Jet Transport Aircraft, Volume 1: Mathematical Model*, NASA Report [NASA CR-1756], NASA, Washington, DC, March.

Klyde, D., Magdaleno, R. and Reinsberg, J. (2002), "The effect of tire pressure on aircraft ground handling", paper presented at AIAA Atmospheric Flight Mechanics Conference and Exhibit, Monterey, California, AIAA Paper 2002-4798.

Mazur, D. (2002), "The X-47A Pegasus: from design to flight", paper presented at 1st UAV Conference, Portsmouth, Virginia, AIAA Paper 2002-3426.

Medici, G., Viola, N., Corpino, S. and Fioriti, M. (2012), "Development and validation of on-board systems control laws", *Aircraft Engineering and Aerospace Technology*, Vol. 84 No. 3, pp. 151-61.

Pacejka, H.B. (2006), *Tyre and Vehicle Dynamics*, Elsevier, Oxford.

Pradeep, S. (2002), "Nonlinear control of unmanned combat aircraft during take-off", paper presented at AIAA 40th Aerospace Sciences Meeting and Exhibit, Reno, NV, AIAA Paper 2002-0250.

Rankin, J. (2010), "Bifurcation analysis of nonlinear ground handling of aircraft", PhD thesis, University of Bristol, Bristol, March.

Stevens, B.L. and Lewis, F.L. (2003), *Aircraft Control and Simulation*, Wiley, Hoboken, NJ.

Wang, J.S. (2001), "Nonlinear control theory and its application to aircraft antiskid brake systems", PhD thesis, Northwestern Polytechnical University, Xi'an.

Wise, K. (2003), "X-45 program overview and flight test status", paper presented at 2nd AIAA Unmanned Unlimited Conference and Workshop and Exhibit, San Diego, CA, AIAA Paper 2003-6645.

Xiong, H., Jing, F.S., Yi, J.Q. and Fan, G.L. (2009), "Automatic takeoff of unmanned aerial vehicle based on active disturbance rejection control", *Proceedings of the 2009 IEEE International Conference on Robotics and Biomimetics, Guilin, IEEE*, pp. 2474-9.

York, W. and Alaverdi, O. (1996), "A physically representative aircraft landing gear model for real-time simulation", *AIAA Flight Simulation Technologies Conference, San Diego, CA*, AIAA Paper 96-3506, pp. 286-92.

Yuan, Z.H. and Wang, Y. (2009), "A design of airplane's integrated ground directional system with fuzzy control", *Sixth International Conference on Fuzzy Systems and Knowledge Discovery, Tianjin, IEEE*, pp. 13-17.

Zhang, X.Y., Duan, H.B. and Yu, Y.X. (2010), "Receding horizon control for multi-UAVs close formation control based on differential evolution", *Science China Information Sciences* (*Science in China Series F*), Vol. 53 No. 2, pp. 223-35.

Zhao, Z.Y. and Lu, G.S. (2012), "Receding horizon control for cooperative search of multi-UAVs based on differential evolution", *International Journal of Intelligent Computing and Cybernetics*, Vol. 5 No. 1, pp. 145-58.

Appendix

The linear lateral-directional model which is linearized at a forward speed of 100 ft/s is shown as follows.

The linear lateral-directional model is given by:

$$\Delta\dot{X} = A\Delta X + B\Delta U \tag{A1}$$

where:

$$\Delta X = (\Delta v_{by}, \Delta p, \Delta r, \Delta\psi, \Delta\phi, \Delta y, \Delta\omega_{ml}, \Delta\omega_{mr})^T \tag{A2}$$

$$\Delta U = (\Delta\delta_r, \Delta\theta_{nws}, \Delta M_{bml}, \Delta M_{bmr}, \Delta V_w, \Delta\delta_a)^T \tag{A3}$$

$$A = \begin{pmatrix} -1.927 & 1.016 & -97.583 & 0 & -0.127 & 0 & 0 & 0 \\ 0.687 & -29.784 & 3.547 & 0 & -114.266 & 0 & -0.015 & 0.015 \\ -0.008 & 0.400 & -0.741 & 0 & 1.624 & 0 & 0.094 & -0.094 \\ 0 & 0 & 1.000 & 0 & 0 & 0 & 0 & 0 \\ 0 & 1 & 0.008 & 0 & 0 & 0 & 0 & 0 \\ 1 & 0 & 0 & 100 & -0.827 & 0 & 0 & 0 \\ 0 & 8.903 & 0.073 & 0 & 44.515 & 0 & -22.139 & 0 \\ 0 & -8.903 & -0.073 & 0 & -44.515 & 0 & 0 & -22.139 \end{pmatrix} \tag{A4}$$

$$B = \begin{pmatrix} 1.947 & 44.925 & 0 & 0 & 0.076 & -0.160 \\ 0.234 & -17.604 & 0 & 0 & 0.015 & -0.842 \\ -0.179 & 3.694 & 0 & 0 & -0.002 & 0.025 \\ 0 & 0 & 0 & 0 & 0 & 0 \\ 0 & 0 & 0 & 0 & 0 & 0 \\ 0 & 0 & 0 & 0 & 0 & 0 \\ 0 & 0 & -0.00035 & 0 & 0 & 0 \\ 0 & 0 & 0 & -0.00035 & 0 & 0 \end{pmatrix} \tag{A5}$$

The approximate directional model extracted from the above complete model is given by:

$$\Delta\dot{X}_d = A_d\Delta X_d + B_d\Delta U_d \tag{A6}$$

where:

$$\Delta X_d = (\Delta v_{by}, \Delta r, \Delta\psi, \Delta y)^T \tag{A7}$$

$$\Delta U_d = (\Delta\delta_r, \Delta\theta_{nws}, \Delta M_{bml}, \Delta M_{bmr}, \Delta V_w, \Delta\delta_a)^T \tag{A8}$$

$$A_d = \begin{pmatrix} -1.928 & -97.6 & 0 & 0 \\ 0.003937 & -0.6785 & 0 & 0 \\ 0 & 1.0 & 0 & 0 \\ 0.995 & -0.02746 & 100.0 & 0 \end{pmatrix} \tag{A9}$$

$$B_d = \begin{pmatrix} 1.947 & 44.95 & -2.655\times10^{-10} & 2.655\times10^{-10} & 0.07607 & -0.1592 \\ -0.1756 & 3.386 & -1.501\times10^{-6} & 1.501\times10^{-6} & -0.00231 & 0.01043 \\ 0 & 0 & 0 & 0 & 0 & 0 \\ -0.001696 & 0.1274 & -1.724\times10^{-9} & 1.724\times10^{-9} & -0.0001145 & 0.006101 \end{pmatrix} \tag{A10}$$

Aircraft Engineering and Aerospace Technology: An International Journal
Volume 85 · Number 1 · 2013 · 48–61

The approximate roll model extracted from the complete model is given by:

$$\Delta \dot{X}_r = A_r \Delta X_r + B_r \Delta U_r \tag{A11}$$

where:

$$\Delta X_r = (\Delta p, \Delta \phi)^T \tag{A12}$$

$$\Delta U_r = (\Delta V_w, \Delta \delta_a)^T \tag{A13}$$

$$A_r = \begin{pmatrix} -29.8 & -114.3 \\ 1.0 & 0 \end{pmatrix} \tag{A14}$$

$$B_r = \begin{pmatrix} 0.01583 & -0.8429 \\ 0 & 0 \end{pmatrix} \tag{A15}$$

About the authors

Yunpeng Zhang is currently a Master student with the Science and Technology on Aircraft Control Laboratory, School of Automation Science and Electrical Engineering, Beihang University, Beijing, PR China. His current research interest is advanced flight control, and intelligent information processing.

Haibin Duan is currently a Professor and PhD advisor with the Science and Technology on Aircraft Control Laboratory, School of Automation Science and Electrical Engineering, Beihang University, Beijing, PR China. His current research interests are bio-inspired computation, advanced flight control, and bio-inspired computer vision. Haibin Duan is the corresponding author and can be contacted at: hbduan@buaa.edu.cn